On the wind advection influence on the fire spread across a fuel bed: modelling by a semi-physical approach and testing with experiments

On the Wind Advection Influence on the Fire Spread Across a Fuel Bed Modelling by a Semi-Physical Approach and Testing with Experiments

A. Simeoni [*] [(1)], P.A. Santoni [(1)], M. Larini [(2)] and J.H. Balbi [(1)]

[(1)] SPE – CNRS UMR 6134, Campus Grossetti, Università di Corsica

[(2)] IUSTI – CNRS UMR 6595, Technopôle de Château-Gombert

ABSTRACT

This paper is devoted to the study of the advection effect on the fire spread across a fuel bed by means of a semi-physical model. This work is a step forward in our general process which consists in elaborating a simple model of fire spread to be used in a simulator. To this end, a thermal balance including an advective term coupled with a wind velocity profile in the burning zone is presented. Following our general procedure that consists in using the multiphase approach to elaborate our semi-physical model, we used the momentum equation of the multiphase model to set this wind profile. The predictions of the model were then compared to experimental data obtained for fire spread conducted across pine needle litters. Different slope values and varying wind velocities were considered. The experimental tendency for the variation of the rate of spread was predicted, especially for the higher values of wind.

Keywords: Fire spread, advection influence, multiphase model, semi-physical model.

[*]e-mail: simeoni@univ-corse.fr, Phone: 00 (33) 4 95 45 01 61, Fax: 00 (33) 4 95 45 01 62

NOMENCLATURE

A	constant in the wind profile
c	rate of spread
C_p	specific heat at constant pressure
d	prevalence distance of the radiant heat flux
e	total energy
$\vec{F}$	drag forces
$\vec{g}$	acceleration due to gravity
$\vec{i}, \vec{j}, \vec{k}$	unity vectors in space
$\overline{\overline{I}}$	unity tensor
k	reduced heat transfer coefficient
k_v	reduced advection coefficient
k_v^*	constant in the k_v expression
K	thermal diffusivity
L	heat of vaporisation
m	surface thermal mass
$\dot{M}$	mass flux
p	pressure
P	reduced radiative coefficient
q	heat flux
Q	reduced combustion enthalpy
R	radiant flux
t	time

T temperature

$\vec{V}$ velocity

$\vec{V}_{\infty}$ maximal wind velocity

x, y, z coordinates of a point in space

Y mass fraction of a chemical species

Greek symbols

α volume fraction

β slope angle

γ combustion time constant

Γ rate of production of a chemical species at the solid / gas interface

δ thickness of the fuel layer

ΔH reaction enthalpy of solid phases

θ angle located between the normal of the front and the direction of spread

λ thermal conductivity

$\overline{\overline{\pi}}$ stress tensor in the gas

$\vec{\Pi}$ stresses at the solid / gas interface

ρ density

σ surface mass

ϕ flame tilt angle

$\dot{\omega}$ species mass rate of production

Ω domain of calculation

$\vec{\nabla}_s$ surface divergence vector

Diacriticals

$[\ ]$	source term
$\|\ \|$	Euclidean value

Subscripts

a	ambient
g	gaseous phase
gk	interface exchanges
ig	ignition
k	solid phase
q	queue of the fire front
s	surface component of a vector
0	initial condition

superscripts

eq	medium equivalent to the litter
i	chemical species i
pr	gaseous products
$surf$	surface regression
δ	value at the top of the bed

INTRODUCTION

Forest fire spread modelling deals with several different approaches. Following the classification of Weber [1], one can define three kinds of modelling. The simplest models are the statistical ones which make no attempt to involve physical mechanisms [2]. Otherwise, the empirical models [3], are based upon the conservation of energy but they do not distinguish the modes of heat transfer. Finally, the physical models differentiate among the various kinds of heat transfer in order to predict the fire behaviour [4,5]. Among these, the multiphase modelling which takes into account the detailed physical phenomena involved in fire spread represents the most complete approach that has been developed so far [6,7,8].

The aim of our research team is to create an operational management tool which is able to describe the spread of a forest fire in order to help fire fighters to make the appropriate decisions. Most of the disastrous forest fires that occurred in the last few years (Catalunya, United States, Corsica, etc…) were associated with high winds. Therefore, it is crucial for the fire fighting teams to possess the means of prediction. It is necessary for a simulator to represent correctly the fire behaviour in such situations, and to allow short calculation times so as to give the information about the spreading in the shortest possible time. Thus, these kinds of tools necessitate simple and robust models.

In a previous study [9], we have developed as a basis towards our aim, a two-dimensional model of fire spread across a fuel bed which will be recalled for reasons of clarity. This last approach was inspired by the diffusion-reaction equation and allowed us to determine, from a single equation, the main characteristics of a laboratory-scale litter fire under windless and slopeless conditions. This model and its evolution can be classified as semi-physical. Indeed, the main heat transfer mechanisms are differentiated in this

formulation and the model's parameters, which are fuel dependent, are obtained from the fire dynamical behaviour. In a second paper, this model was improved in order to include the slope effect [10]. Then, one attempt was to consider the wind influence by assuming a similar effect of wind and slope due only to radiating flame heat transfer [11]. Although this derived model was able to predict both strong slope and combined slope and low wind effects, it failed to describe the fire behaviour with increasing wind velocity.

In recent work, we have developed a theoretical method of improvement of semi-physical models thanks to a multiphase approach [12]. This study has proved the necessity of including an advection term in our model. The addition of this term was in accordance with several works which have demonstrated that, from a certain wind velocity, the advection cannot be neglected in front of the radiative transfer [13,14]. The advective term was modelled in a simple manner however (constant wind velocity onto the whole domain of spread). And it did not represent correctly the experimental tendency even if it brought to the fore the necessity of considering the wind influence. So, we deduced that it was necessary to take into account the variation of the gas velocity in the burning zone. Hence, the present paper is devoted to the improvement of our model to take better account of the coupling between the wind and the thermal balance. To proceed, we used the momentum equation of the multiphase model to set the wind profile. Indeed, as this approach is inspired by a complete model [8], it permits us to control the different simplifications and to determine the weaknesses if necessary.

The first section presents the multiphase model and its reduction which is used to improve our semi-physical model. The semi-physical model, its improvement, which takes into account the wind advection, and the setting of the reduced wind profile to be coupled to the model are detailed in the second section. The numerical method used to solve the temperature equation of our model is then presented in the third section. The fourth section

is devoted to the presentation of the experimental method that was used to validate the results of the model. The last section concerns the comparison of the results of the model with experimental data and the discussion. To this end, different slopes and varying wind velocities are considered for fire spread conducted across pine needle fuel beds.

1. THE MULTIPHASE APPROACH

The complete model

As the bases of this model have already been presented [8], only the essential features of this work are provided here. The aim of this approach is to represent the fire spread medium as a reactive and radiative multiphase one. This medium is defined by the fluid phase and *N* solid phases. Each solid phase consists in a set of particles which possess the same geometry and thermochemical properties. An elementary multiphase volume is defined to carry out averaged properties of both gaseous and solid phases. This last volume should be considered as smaller than the scale of the phenomenon but greater than the size of the particle. The whole set of multiphase equations governing the previous averaged properties is obtained in two steps. Firstly, point equations for the fluid and for the fuel phases as well as the interface conditions are established by using Delaye's formulation [15]. Secondly, this set of equations is space averaged applying Anderson and Jackson's approach [16] to the multiphase medium. Finally, we obtain the system of averaged equations presented hereafter. For the sake of clarity, symbols identifying that the variables are volume averaged have been omitted:

Gas phase:

Mass equation

$$\frac{\partial}{\partial t}\left(\alpha_g \rho_g\right) + \vec{\nabla}.\left(\alpha_g \rho_g \vec{V}_g\right) = \sum_k \left[\dot{M}\right]_{gk} \tag{1}$$

Chemical species equation

$$\frac{\partial}{\partial t}\left(\alpha_g \rho_g Y_g^i\right) + \vec{\nabla}.\left(\alpha_g \rho_g Y_g^i \vec{V}_g\right) + \vec{\nabla}.\left(\alpha_g \rho_g Y_g^i \vec{V}_g^i\right) - \alpha_g \rho_g \dot{\omega}_g^i = \sum_k \left[\dot{M}\right]_{gk}^i \tag{2}$$

Momentum equation

$$\frac{\partial}{\partial t}\left(\alpha_g \rho_g \vec{V}_g\right) + \vec{\nabla}.\left(\alpha_g \rho_g \vec{V}_g \vec{V}_g\right) - \vec{\nabla}.\left(\alpha_g \overline{\overline{\pi}}_g\right) - \alpha_g \rho_g \vec{g} = \sum_k \left[\dot{M}\vec{V}\right]_{gk} + \sum_k \left[\vec{\Pi}\right]_{gk} \tag{3}$$

Total energy equation

$$\begin{aligned} &\frac{\partial}{\partial t}\left(\alpha_g \rho_g e_g\right) + \vec{\nabla}.\left(\alpha_g \rho_g e_g \vec{V}_g\right) + \vec{\nabla}.\left(\alpha_g \left(\vec{q}_g + \vec{R}_g\right)\right) - \vec{\nabla}.\left(\alpha_g \overline{\overline{\pi}}_g.\vec{V}_g\right) \\ &- \alpha_g \rho_g \vec{g}.\vec{V}_g = \sum_k \left[\dot{M}e\right]_{gk} - \sum_k \left[q\right]_{gk} - \sum_k \left[R\right]_{gk} + \sum_k \left[\vec{\Pi}.\vec{V}\right]_{gk} \end{aligned} \tag{4}$$

Solid Phase (*N* equations, one per *k* phase):

Mass equation

$$\frac{\partial}{\partial t}\left(\alpha_k \rho_k\right) = -\left[\dot{M}\right]_k^{surf} - \left[\dot{M}\right]_k^{pr} \tag{5}$$

Chemical species equation

$$\frac{\partial}{\partial t}\left(\alpha_k \rho_k Y_k^i\right) = -\left[\dot{M}\right]_k^{surf,i} - \left[\Gamma\right]_k^{surf,i} - \left[\dot{M}\right]_k^{pr,i} \tag{6}$$

Total energy equation

$$\frac{\partial}{\partial t}\left(\alpha_k \rho_k e_k\right) = -\left[\dot{M}e\right]_k^{surf} - \left[\dot{M}e\right]_k^{pr} - \left[q\right]_k - \left[R\right]_k + \left[\vec{\Pi}.\vec{V}\right]_k^{pr} \tag{7}$$

It should be noticed that no momentum equation appears in the solid phase because it is assumed that each solid phase is motionless. To close the mathematical problem, interface equations are added, and a radiative equation is included to express the radiative contribution in the equation of energy of the different phases (Eqs. 4 and 7). From this method, different sub-models appear in the right hand side of the previous balance equations that should be determined. These last sub-models and the interface equations as well as the radiative transfer equation are not detailed here for clarity, but the interested reader is referred to [8]. This approach has been reduced in order to propose a method for improvement of semi-physical forest fire spread models. Indeed, the three-dimensional model presented here, which takes into account the finest mechanisms involved in fire

behaviour, is not appropriate at the present time to be integrated in fire spread simulators since it needs considerable calculation time. To avoid this disadvantage, we have developed a two-dimensional semi-physical model, based on a single thermal balance, as well as a method to improve it. This method involves the reduction of the complete multiphase model and will be presented hereafter. It leads to a simplified multiphase formulation which nears our semi-physical one (while keeping significant physical information), and which can be used to improve it.

The reduced model

The multiphase model reduction has been carried out in three steps. Firstly, as the semi-physical model is two-dimensional, we reduced the three dimensional multiphase set of equations to two dimensions applying an averaging procedure on the *z*-dimension along δ, the height of the fuel layer (cf. figure 1). For clarity, no symbol indicating that the variables are averaged are included in the following equations. Secondly, since the semi-physical models are generally characterised by a single energy conservation equation, the thermal balances of the multiphase model has been reduced to one single equation by means of the thermal equilibrium assumption. Finally, the resulting conservation equation of energy has been expressed in term of temperature by using the previous set of reduced equations. The last result will be used to improve our semi-physical model.

After making calculations and setting some hypothesis of reduction, we obtained the following equation in which pressure, stress, gravity and conduction contributions are neglected and a single solid phase is considered [12]:

$$\begin{aligned}&\left(\alpha_g \rho_g C_{p,g} + \alpha_k \rho_k C_{p,k}\right)\frac{\partial T}{\partial t} + \alpha_g \rho_g C_{p,g} \vec{V}_{g,s}.\vec{\nabla}_s T + \alpha_g \rho_g C_{p,g} V_{g,z} \frac{\left[T\right]_0^\delta}{\delta} \\ &+ \vec{\nabla}_s.\left(\alpha_g \vec{R}_{g,s}\right) + \frac{\left[\alpha_g R_{g,z}\right]_0^\delta}{\delta} = -\left[\dot{M}\right]_k^{pr} L^{pr} - \left[\dot{M}\right]_k^{surf} \Delta H^{surf} - \sum_i \alpha_g \rho_g \dot{\omega}_i h_g^i\end{aligned} \tag{8}$$

This equation represents the mean mechanisms of propagation like convection, radiation and reactions. Furthermore, it is expressed in a form that enables resolution through the expression of appropriate sub-models. It should be borne in mind that Eq. 8 is only a part of the whole reduced multiphase model which is derived from Eqs. 1 to 7.

Among these equations, the momentum equation is provided below as it will be used to set the wind profile to be coupled with the semi-physical model. This equation is derived from the momentum equation of the complete model (Eq. 3), on which we have applied the averaging operation along δ.

So, we obtain the following equation:

$$\frac{\partial}{\partial t}\left(\alpha_g\ \rho_g\ \vec{V}_g\right)+\vec{\nabla}_s.\left(\alpha_g\ \rho_g\ \vec{V}_g\ \vec{V}_{g,s}\right)+\frac{\left[\alpha_g \rho_g \vec{V}_g V_{g,z}\right]_0^\delta}{\delta}+\vec{\nabla}_s.\left(\alpha_g\ \overline{\overline{\pi}}_{g,s}\right)+\frac{\left[\alpha_g \vec{\pi}_{g,z}\right]_0^\delta}{\delta}= \alpha_g\ \rho_g\ \vec{g}+\left[\dot{M}\vec{V}_{g,s}\right]_{gk}+\frac{\left[\dot{M}\ \vec{V}_{g,z}\right]_0^\delta}{\delta}+\left[\vec{\Pi}_{g,s}\right]_{gk}+\frac{\left[\vec{\Pi}_{g,z}\right]_0^\delta}{\delta} \quad (9)$$

Where: $-\left[\dot{M}\vec{V}_{g,s}\right]_{gk}+\frac{\left[\dot{M}\ \vec{V}_{g,z}\right]_0^\delta}{\delta}$ is the momentum of the gaseous products released by the solid phase (vaporisation and pyrolysis) at the solid / gas interface.

$-\left[\vec{\Pi}_{g,s}\right]_{gk}+\frac{\left[\vec{\Pi}_{g,z}\right]_0^\delta}{\delta}$ represents the stresses at the interface between the gas and solid phases.

This reduced model remains too far from our aim which is to elaborate a simple model which can be used as an operating management tool. It can be considered as a useful tool of improvement of semi-physical models however. Thus, Eq. 8 will be compared with the semi-physical model presented hereafter, so as to improve it. And Eq. 9 will be used to set the wind profile.

2. THE SEMI-PHYSICAL MODELLING

The semi-physical model

The aim of our research team is to develop a simple fire spread model to be used as an operational management tool. Due to the amount of physical phenomena and state variables involved in fire behaviour, it is necessary to make some simplifying hypotheses in order to generate a comprehensive and simple model. These hypotheses lead us to combine these physical phenomena and to consider a thermal balance which provides the framework of the model. In order to write it, elementary cells composed of soil and plant matter are defined. As a whole, these cells are considered to represent a thin, isotropic and homogenous medium equivalent to the litter. The energy transferred from a cell to the surrounding air is considered to be proportional to the difference between the temperature of a cell and the ambient temperature. Combustion reaction is assumed to occur above a threshold temperature (T_{ig}). Above this threshold, the fuel mass decreases exponentially and the quantity of heat generated per unit fuel mass is constant. The heat transferred between a cell and its neighbouring cells is due to three mechanisms: radiation, convection and conduction. We assumed that these exchanges can be represented by a single equivalent diffusion term, under no slope and no wind condition. However, due to obvious geometric reasons, a supplementary radiation was considered for an up-slope fire [10]. The following hypotheses are proposed in order to evaluate it:

- We consider the flame to be a vertical radiant surface (cf. figure 2), at least up to a limit angle [17].
- We assume that the radiant heat flux prevails over a short distance d (in the calculation performed in this paper, d is equal to the spatial increment value of 0.01 m).

- We consider that the flame temperature T is equal to the temperature of the burning cell located below it. This temperature is given by the model. By using a Stefan-Boltzmann law, we assume that the radiant heat flux is proportional to T^4.

By using these hypotheses, the supplementary radiation was determined in Santoni et al. [10]. From this analysis, it is shown that an unburned cell in the direction of the slope receives an additional radiant heat flux from an burning cell directly before it which is proportional to the cosine of the angle θ located between the normal of the front and the direction of the slope. Hence, when all of the previous assumptions are considered, we obtain:

$$R = P(\phi)\cos(\theta)T^4(x-d,y,t) \tag{10}$$

where $T(x-d,y,t)$ is the temperature of the burning cell located before the unburned cell under consideration, with $P(\phi)$ being a function of the slope angle, the emissivity of the flame, the absorptivity of the fuel and the view factor. It is not reasonable to take all of these parameters into consideration in our macroscopic approach. P will therefore be determined by using the following considerations:

- For horizontal and down-slope fires the flame lean backward and $P(\phi)=0$ which means that there is no supplementary radiant effect.
- Based on laboratory fire experiments of Mendes-Lopes et al. [18], we established an analogy between the fire behaviour under slope and wind condition when flame tilt angle is below a threshold value [11]. $P(\phi)$ is then a function of the flame tilt angle under up-slope and wind-aided conditions ϕ (cf. figure 2).
- P was fitted for each slope in accordance with the rate of spread and we deduced the following relation by a least squares approximation [11]:

$$P(\phi) = p^* \sin^4(\phi) \tag{11}$$

where p^* is a constant which value will be provided later. This relation has been used directly in the present paper to obtain the values of *P*.

With regard to ϕ, a simple relation was used to determine it: this angle was considered as the composition of the tilt angle due to the slope (equal directly to the slope angle β) and the tilt angle due to the wind effect (predicted as a composition of the wind velocity and the buoyancy flow velocity, taken both at mid-flame, which was determined in Morandini et al. [11]).

Thus, we obtained the following model of fire spread:

$$\frac{\partial T}{\partial t} = -k(T - T_a) + K\Delta T - Q\frac{\partial \sigma_k}{\partial t} + R \qquad \text{on the fuel complex} \tag{12}$$

with the conditions presented here:

$R = 0, \quad \sigma_k = \sigma_{k0} e^{-\gamma(t - t_{ig})}$	for a burning cell
$R = P(\phi)\cos(\theta)T^4(x - d, y, t), \quad \sigma_k = \sigma_{k0}$	for an inert cell ahead of the fire front
$R = 0, \quad \sigma_k = \sigma_{k0}$	for an unburned cell elsewhere
$T = T_a$	at the boundaries far from the fire
$T(x, y, t = 0) = T_a$	for an unignited cell at time zero
$T(x, y, t = 0) = T_{ig}$	for an ignited cell at time zero

where t_{ig} is the time for which $T = T_{ig}$.

The model parameters (*k, K, Q* and γ) are determined using the experimental temperature measurements over time for a fire spreading in a linear way [9]. Due to our approach, these parameters are fuel-dependent and must therefore be identified for each fuel. Thus, the usual fuel descriptors such as mass per unit area, particle size, compactness, physico-chemical properties and moisture content are intrinsically taken into account.

This model, which will be called the radiative model, remained valid for a combined slope and low wind velocity $\left(\leq 1 m s^{-1}\right)$, but it was not able to predict the fire behaviour under higher wind velocities. In order to obtain a better representation of the spreading

above this threshold, we used the reduced multiphase model to propose an improvement of our formulation as presented in the following section.

The advective and radiative model

By comparing Eq. 12 to Eq. 8, we can see that the essential aspects of the fire spread behaviour are represented, except one in Eq. 12. Indeed, both models consider chemical kinetic, radiant and convective heat transfer. The main difference between the two formulations consists in the advection contribution which was omitted in our model:

$$\alpha_g \rho_g C_{p,g} \vec{V}_{g,s} . \vec{\nabla}_s T \tag{13}$$

Hence, we proposed to add this term in the semi-physical model (Eq. 12), which becomes:

$$\frac{\partial T}{\partial t} + k_v \vec{V}_g . \vec{\nabla} T = -k(T - T_a) + K\Delta T - Q\frac{\partial \sigma_v}{\partial t} + R, \tag{14}$$

The added term should be discussed in order to provide an appropriate formulation for the gas velocity $\vec{V}_g$ and to identify the coefficient k_v. With regard to $\vec{V}_g$, we assumed as a first step that the maximum wind velocity $\vec{V}_\infty$ can be used in Eq. 14 to take roughly into account the wind influence on the propagation. Hence, we called this variant the constant-wind model. The coefficient k_v was deduced from the multiphase model, assuming in addition that the gas is perfect, its specific heat remains constant and the quasi – isobaric approximation is valid. So, we obtain the following relation [12]:

$$k_v = k_v^* \cdot \frac{T_a}{T} \tag{15}$$

Where k_v^* is a constant, and is equal to:

$$k_v^* = \frac{\alpha_g \rho_a \delta C_{p,g}}{m_{eq}} \tag{16}$$

in which m_{eq} is the surface thermal mass of the semi-physical medium equivalent to the litter.

As the assumption of the wind velocity equal to $\vec{V}_\infty$ has proved to be too crude to enable a good prediction of the spreading [12], we decided to include a wind profile to take into account the variation of the gas velocity in the burning zone.

Including a reduced wind profile

To be in accordance with our approach which consists of using the multiphase model to improve our semi-physical formulation, we used the reduced multiphase momentum equation (Eq. 9) to set the reduced wind profile. As a first stage, in order to evaluate the effect of coupling a wind profile with our thermal balance, a simple configuration will be studied in which Eq. 9 will be simplified to derive the gas velocity. Indeed, in order to allow a short calculation time and following our needs (elaborating a simulator), a simple wind profile will be a relevant sub-model to couple with our thermal balance carrying out the wind effects. The simplification of the momentum equation is managed by setting the following assumptions:

- We neglect the momentum of the gaseous products released by the solid phase as well as the viscous stress in the volume of the gas and the pressure at the interface between solid and gas phases. So, the stress tensor in the gas is reduced to:

$$\bar{\bar{\pi}}_g = -p_g \bar{\bar{I}} \tag{17}$$

And the stress at the interface between the solid and the gas phases is reduced to the drag forces:

$$\left[\vec{\Pi}_{g,s}\right]_{gk} + \frac{\left[\vec{\Pi}_{g,z}\right]_0^\delta}{\delta} = \left[\vec{F}_{g,s}\right]_{gk} + \frac{\left[\vec{F}_{g,z}\right]_0^\delta}{\delta} \tag{18}$$

Thus, we obtain the following equation:

$$\frac{\partial}{\partial t}\left(\alpha_g \rho_g \vec{V}_g\right) + \vec{\nabla}_s.\left(\alpha_g \rho_g \vec{V}_g \vec{V}_{g,s}\right) + \frac{\left[\alpha_g \rho_g \vec{V}_g V_{g,z}\right]_0^\delta}{\delta} + \vec{\nabla}_s.\left(\alpha_g p_g\right) + \frac{\left[\alpha_g p_g \vec{k}\right]_0^\delta}{\delta} = \alpha_g \rho_g \vec{g} + \left[\vec{F}_{g,s}\right]_{gk} + \frac{\left[\vec{F}_{g,z}\right]_0^\delta}{\delta} \tag{19}$$

- In this first stage, we only consider the wind velocity in the direction of the spreading, $V_{g,x}$ (x coordinate). It should be noticed that $V_{g,x}$ represents the mean value of the horizontal velocity (in the x direction) over the height of the litter. Thus, the reduced wind profile concerns here the variation of the horizontal velocity in the direction of the spreading. With regard to our two-dimensional model, the variation of the state variables along y is necessary in the general formulation, but it will not be considered at the present time. Indeed, in the fifth section, we will validate our approach thanks to an experimental device which allows this hypothesis to be formulated. By subtracting the reduced mass balance (deduced from Eq. 1) from Eq. 19, and by considering solely the governing equation along x, we obtain:

$$\begin{aligned}&\alpha_g\,\rho_g\,\frac{\partial V_{g,x}}{\partial t}+\alpha_g\,\rho_g\,V_{g,x}\,\frac{\partial V_{g,x}}{\partial x}+\alpha_g\,\rho_g V_{g,z}\,\frac{\left[V_{g,x}\right]_0^{\delta}}{\delta}+\frac{\partial}{\partial x}\left(\alpha_g\,p_g\right)=\\&-\alpha_g\,\rho_g\,g\sin\beta+\left[F_{g,x}\right]_{gk}-\left[\dot{M}\right]_{gk}V_{g,x}\end{aligned}\tag{20}$$

where β is the slope angle.

- Buoyancy, drag forces and $V_{g,z}$ contributions are supposed to be equivalent to a force proportional to the quantity of the gas present in the multiphase volume solely and acting on the gas when it penetrates the fire plume:

$$\begin{aligned}&-\alpha_g\,\rho_g V_{g,z}\,\frac{\left[V_{g,x}\right]_0^{\delta}}{\delta}-\frac{\partial}{\partial x}\left(\alpha_g\,p_g\right)-\alpha_g\,\rho_g\,g\sin\beta\\&+\left[F_{g,x}\right]_{gk}-\left[\dot{M}\right]_{gk}V_{g,x}=-\alpha_g\,\rho_g\,A\end{aligned}\tag{21}$$

Where A is a constant representing the forces acting on the gas.

So, Eq. 20 becomes:

$$\alpha_g\,\rho_g\,\frac{\partial V_{g,x}}{\partial t}+\alpha_g\,\rho_g\,V_{g,x}\,\frac{\partial V_{g,x}}{\partial x}=-\alpha_g\,\rho_g\,A\tag{22}$$

This hypothesis assumes that the action of all the different forces remains constant whatever the gas velocity is, and that the change of $V_{g,x}$ due to $V_{g,z}$ is constant. We thus consider that the variation of $V_{g,x}$ is due to a global force that is difficult to model accurately and whose effect is to decrease $V_{g,x}$ value when the gas enters the fire plume. It is certainly a big assumption, but the interest of this approach is to demonstrate that the knowledge of the variation of the gas velocity in the burning zone is essential for our model and brings a substantive improvement to the prediction of the rate of spread. The parameter *A* is adjusted once and remains the same for all the other configurations of slope and wind. It should be noticed that its value will determine whether the flow passes through the flame, or is stopped by it. In order to solve Eq. 22 we further assume that:

- The velocity $V_{g,x}$ at the entering of the burning zone, is equal to $\left\|\vec{V}_{\infty}\right\|$ and decreases uniformly to zero throwing it (queue of the front to ignition interface in figure 3). We neglect the aspiration of cold gas ahead of the flame.
- The flow is assumed quasi-steady, i.e. the profile remains constant into an elementary interval of time associated to the thermal balance and must be recalculated at each time step. Thus, the time rate of change of the velocity in Eq. 22 is neglected and we obtain the following simplified equation (that follows the burning zone):

$$V_{g,x}\frac{\partial V_{g,x}}{\partial x} = -A \tag{23}$$

Finally, we can set the wind profile along *x*:

$$V_{g,x}(x) = V_{\infty}\sqrt{1-\frac{2A(x-x_q)}{V_{\infty}^2}} \tag{24}$$

Where x_q is the coordinate of the queue of the front.

Eq. 24 will be used as a sub-model to determine the gas velocity present in the advective term of our model (Eq. 14).

3. NUMERICAL METHOD

We used a numerical method to solve Eq. 14. Indeed, analytical solutions exist for simple fire spread models [19], but generally, a numerical approach is necessary to study mathematical problems. Tang and Weber [20], studied a two-dimensional reaction-diffusion equation numerically, using the finite element and finite difference methods. The finite difference scheme was examined in the present study and is presented here.

The computational domain Ω is divided into a rectangular grid. The Laplacian of T at the inner grid nodes is estimated by central finite differences which have a second order accuracy in space. And the time rate of change of T is approximated by right finite differences which have a first order accuracy. For the added advective term an upwind-difference scheme has been used in order to take into account the importance of the gas transfers in the wind direction [21].

Eq. 14 is discretised onto the domain Ω and leads to a linear system which is solved using the Jacobi iterative method [22]. The homogeneous grid used is relatively fine with a mesh size of 0.01 m and the time step is 0.01 s.

4. EXPERIMENTAL FACILITY AND PROCEDURE

Experimental set-up

The experiments were carried out in a dedicated low speed wind tunnel, as depicted in figure 4, at *Instituto Superior Técnico* of Lisboa [18]. They were performed in order to

observe wind driven fire across fuel beds of pine needles. Furthermore, the tunnel allows slope effects to be studied with a sloping fuel tray (cf. figure 4).

The wind speed values covered the range between $-3\ m\ s^{-1}$ and $3\ m\ s^{-1}$. The movable tray can be set at angles from *0* up to *15°* with up-slope and down-slope orientation. The fuel bed occupies the central part of the tray (*0.70 m* wide). It consists of a layer of *Pinus pinaster* needles, attempting to reproduce a typical layer found in Portuguese stands, with a load of approximately $0.5\ kg\ m^{-2}$ on dry basis and a fuel moisture content of $(10 \pm 1\%)$.

Experimental runs

The movable tray is positioned at the required angle and the wind velocity is fixed at the required value. The conditioned pine needles are scattered uniformly on the tray. To ensure a fast and linear ignition, a small amount of alcohol and a flame torch are used. The fuel is ignited perpendicularly to the flow, at the wind tunnel side for wind driven fire and at the opposite side for back-wind fire. In order to obtain a uniform and established flame propagation, the fuel bed was ignited sufficiently far away from the work section. Three runs are carried out for each set of conditions. The experimental runs are recorded by video.

Rate of spread, flame geometry and temperature recording

The rate of spread is obtained from the derivative of the curve *"flame front position vs time"*. Twenty to thirty images of each experimental run are analysed in order to determine the mean flame angle which is defined as the angle between the tray and the leading surface of the flame. Temperature measurements were made using K type thermocouples with *250 μm* wire diameter.

5. NUMERICAL RESULTS AND DISCUSSION

Previous results

In the first place, the varying experimental configurations were simulated with the radiative model [11], and with the constant-wind model [12]. The model's dynamical coefficients were determined from experimental temperature curves in slopeless and windless conditions as explained in [9]. So, we obtained the following values:

$$k = 97\times10^{-3}\ s^{-1},\ K = 14.5\times10^{-6}\ m^2\ s^{-1},\ Q = 3.67\times10^{3}\ m^2\ K\ kg^{-1},$$

$$\gamma = 0.234\ s^{-1}, p_0 = 9\times10^{-9}\ K^{-3}\ s^{-1}$$

The predicted and observed temperature profiles (measured at the top of the fuel bed) are provided in figure 5 in slopeless and windless conditions. A general agreement is observed on the envelope of these simulated and experimental curves. We do not detail the results that have already been discussed in Balbi et al. [9].

The predictions for the radiative model and for the constant–wind model are presented in figure 6 for no slope configuration. With regard to the radiative model, the results were in agreement with the experimental data up to a wind velocity of $1 m s^{-1}$ [11]. The model was not able to accurately describe the increase of the rate of spread with the wind velocity, however. Furthermore, the experimental value was poorly represented for the highest wind velocity of $3 m s^{-1}$. The constant-wind model brought a consistent improvement for the prediction [12]. Nevertheless, two values for the coefficient k_v^* were necessary: one to represent correctly the spreading up to wind velocities of $2 m s^{-1}$, $\left(k_v^* = 4\times10^{-3}\right)$, and a further value to represent it for the highest wind velocity of $3 m s^{-1}$, $\left(k_v^* = 11\times10^{-3}\right)$. These results brought to the fore the question of defining a wind profile to

circumvent this weakness; i.e. to keep a unique value of k_v^* (and to represent the variation of the gas velocity in the burning zone).

Contribution of the wind profile

Different configurations were simulated for the range of slope previously presented and for wind velocities $\left\|\vec{V}_\infty\right\|$ of 1, 2 and 3 $m\,s^{-1}$, in order to compare the predictions of the advective and radiative models. The values of the coefficients k, K, Q, γ and p_0 of the model remained the same as presented previously. The value of the constant in the advection term was taken equal to the highest value: $k_v^* = 11 \times 10^{-3}$. Indeed, we could not use the lowest value that underpredicted the rates of spread in the case of wind velocities of 3 $m\,s^{-1}$. On the other hand, the constant A in the wind profile (Eq. 24) was determined so as to obtain the experimental rate of spread in a single case. We used the case of no slope and 2 $m\,s^{-1}$, because it is the median value between 1 and 3 $m\,s^{-1}$. This value remained constant for all the other configurations of slope and wind. We obtained $A = 3.5\,m^{-1}s^2$.

Figures 7 to 9 provide the simulated results, for varying winds under no slope, 5° and 10° upslope configurations respectively. It should be noticed that in figure 7 two experimental rates of spread are superimposed since they were identical for the runs with a 3 m s^{-1} wind velocity. Moreover, two experimental data solely were available for the $2\,m.s^{-1}$ wind velocity runs in figure 9.

We can observe an overall agreement between predicted and observed rates of spread, even if the model underpredicts fire spread for the highest velocity of 3 $m\,s^{-1}$. The agreement is particularly good for all slopes considered when the wind velocity is lower than or equal to 2 $m\,s^{-1}$. A substantial improvement is thus obtained if one considers the previous radiative model which was not able to depict this tendency accurately. Indeed, the

results of the advective model are nearer to the observed one. Moreover, it predicts better the rate of fire spread which increases with increasing wind for a given slope. The highest values of the fire spread rates, for a wind velocity of 3 $m\ s^{-1}$, are better represented than for the radiative model as well. An increase of the predicted rate of spread with increasing slope is also provided, even if it remains lower than the increase of the experimental values. Indeed, although it is correctly given for no slope, conversely it is rather underpredicted for the 5° and 10° slopes.

Two reasons have been found to explain this behaviour. Firstly, the contribution of the advective term remains almost the same while increasing slope for a given wind velocity (same value for the constant k_v^* and same wind profile). No effect of the slope on the increasing advection, like buoyancy, is considered even when the experimental data show this tendency. This disagreement points to the necessity of setting a more detailed wind profile. Indeed, the one-dimensional wind profile used in this study has been obtained by assuming that the action of all the different forces remains constant whatever the gas velocity and the slope are. Although it was a suitable assumption for low winds and slopes, conversely, the same is not true when both slope and wind increase. Further investigations are necessary in order to take into account explicitly important influences like buoyancy (which has intentionally not been addressed here) and to represent the variation of the wind direction that have not been studied yet. This work can be managed by the development of a simple flow model appropriate to our aim (elaborating a simulator).

Secondly, the radiant contribution modelling does not take into account long-range effects (cf. Eq. 12 and its conditions). Figures 10 and 11 give the predicted and observed temperatures profiles at a given point on the top of the fuel bed, and emphasise this weakness. Before discussing these curves, it should be pointed out that the experimental temperature profiles can only be considered qualitatively under wind conditions, as

mentioned in Ventura et al. [23]. Indeed, the coupling of the heterogeneity of the fuel spatial distribution with the turbulent nature of the flow involves some scattering and makes an analysis based on the individual temperature traces difficult. Nevertheless, the general shape can be discussed. Thus, we can see that the envelope of the simulated result matches the experimental one roughly. The peak temperature zone cannot be discussed easily since the thermocouples do not provide accurate values. Indeed, infrared measurements upon the same fuel type [24], reveal that the burning area temperature ranges from 1000°C to 1300°C, that is in accordance with our prediction. The cooling down in the third zone is represented but it cannot be analysed accurately because of the different performances produced by the thermocouples in the same configurations (see also figure 5). As to the preheating zone, the model fails to describe qualitatively the increase of the fuel bed temperature. It should be noticed that the increasing wind velocity stretches and tilts the flame forward in the direction of the unburned fuel and increases the long distance effect of the radiant transfer. This effect can be observed when looking at the figures 5, 10 and 11 in which we see that this influence increases with the wind velocity. The semi-physical model, in which we have assumed a short radiant distance effect by considering that radiation prevails in the inert cell ahead of the fire front, does not perform this last effect. It should be further improved by taking into account the long range radiant heating.

Thus, the under-prediction in the rate of spread for the wind velocity of $3\ m\,s^{-1}$ is a result of the two weaknesses detailed here above (radiant modelling as well as wind profile modelling). Our model will be improved, in order to circumvent them, in future studies based on a theoretical multiphase investigation.

On the other hand, it should be noticed that the wind profiles implied that the hot gases were stopped by the flame for wind velocities less than or equal to $2\,m\,s^{-1}$ and through the

burning zone for the highest winds of $3 m s^{-1}$. These results are in accordance with those of the radiative model which has demonstrated that the radiant effect was dominant for the wind velocities of 1 and $2 m s^{-1}$ but could not explain the increasing of the rate of spread for $3 m s^{-1}$. We also note that, even if the hot gases did not pass through the burning zone for winds of 1 and $2 m s^{-1}$, they involve an increase of its peak temperature (by advection) which causes an increase in the radiant effect on the unburned fuel, to finally induce rates of spread higher than those of the radiative model. On the other hand, it should be noticed that the wind profiles implied that the hot gases were stopped by the flame for wind velocities less than or equal to $2 m s^{-1}$ and through the burning zone for the highest winds of $3 m s^{-1}$. These results are in accordance with those of the radiative model which has demonstrated that the radiant effect was dominant for the wind velocities of 1 and $2 m s^{-1}$ but could not explain the increasing of the rate of spread for $3 m s^{-1}$. We also note that, even if the hot gases did not pass through the burning zone for winds of 1 and $2 m s^{-1}$, they involve an increase of its peak temperature (by advection) which causes an increase in the radiant effect on the unburned fuel, to finally induce rates of spread higher than those of the radiative model.

CONCLUSION

The present work was devoted to the study of the influence of gas velocity on the spreading of flames across a fuel bed under wind conditions. In previous work, our semi-physical model has been improved thanks to a multiphase approach in order to add an advective term in its equation. The present work brought to the fore the question of determining the wind velocity in the flaming zone. The knowledge of the gas velocity

distribution has proved to be essential in our model to represent the rates of spread correctly. Adding a wind profile permitted both a substantive improvement concerning the prediction and using a single value of the advection parameter. Thus, the simplified wind profile presented here has emphasised the necessity of such information, but has proved to be too rough to represent well the gas influence and particularly the buoyancy. To look forward, this study has shown the necessity for the simplified models to be integrated in fire simulators, to model the flow in the fuel layer. Indeed, we have demonstrated in the present work that the temperature was not the single state variable as we supposed firstly while setting our energy equation. The wind velocity must be incorporated as well. Future work, based on the multiphase approach, that contains all the information we need and we have neglected, will be managed in order to obtain a simplified flow model suitable to our aim (to elaborate a simulator) on a more physical basis. Furthermore, the long-range radiant contribution has recently been investigated and will be linked to the model presented in this paper.

Another point which deserves mention is that our model is also capable of providing the front geometry, since it is two-dimensional along the fuel bed. It has been validated both in slopeless and slope configurations, but we could not do the same for the wind-aided spread since we do not possess the contours for the experiments considered here. Thus, further experiments are necessary in order to validate it: this information is of capital importance for the fire fighters, and particularly to co-ordinate their actions in densely populated areas.

ACKNOWELDGEMENTS

The authors would like to thank Pr. Mendes-Lopes, J.M., Pr. Ventura, J.M., Dr. Amaral, J.M. and Dr. Ripado, L.M. for the provided experimental results they have obtained at the IST of Lisboa [18,23].

REFERENCES

[1] Weber, R.O. (1990) Modelling fire spread through fuel beds. *Progress in Energy and Combustion Science* **17**, pp. 67-82.

[2] McArthur, A.G. (1966) Weather and grassland fire behaviour. *Australian Forest and Timber Bureau Leaflet* N° 100.

[3] Rothermel, R.C. (1972) A mathematical model for predicting fire spread in wildland fuels. *United States Department of Agriculture, Forest Service Research*. Paper INT-115. 40 pages.

[4] Albini, F.A. (1985) A model for fire spread in wildland fuels by radiation. *Combustion Science and Technology,* **42**, pp. 229-258.

[5] Weber, R.O. (1991) Toward a comprehensive wildfire spread model. *International Journal of Wildland Fire,* **1** (4), pp 245-248.

[6] Grishin, A.M. (1997) In Albini (Ed.). *Mathematical modeling of forest fires and new methods of fighting them*. Publishing house of the Tomsk state university. Chap. 1. pp. 81-91.

[7] Fan, W. and Wang, J. (1991) Predictions of unsteady burning of a fuel bed. *Proceedings of the 3rd Int. Symp. on Fire Safety Science*, pp. 325-334, Edinburgh.

[8] Larini, M., Giroux F., Porterie B., and Loraud J.C. (1997) A multiphase formulation for fire propagation in heterogeneous combustible media. *International Journal of Heat and Mass Transfer,* **41** (6-7), pp. 881-897.

[9] Balbi, J. H., Santoni, P. A. and Dupuy, J.L. (1999) Dynamic modeling of fire spread across a fuel bed. *International Journal of Wildland Fire*, **9**, pp. 275-284.

[10] Santoni, P. A., Balbi, J. H. and Dupuy, J.L. (1999) Dynamic modelling of upslope fire growth. *International Journal of Wildland Fire*, **9**, pp. 285-292.

[11] Morandini, F., Santoni, P.A., and Balbi, J.H. (2000) Analogy between wind and slope effects on fire spread across a fuel bed – Modelling and validations. *3rd International Seminar on Fire and explosion hazards*. Lake Windermere, 10 – 14 April.

[12] Simeoni, A., Santoni, P.A., Larini, M., and Balbi, J.H. (2000) Proposal for Theoretical Improvement of Semi-Physical Forest Fire Spread Models Thanks to a Multiphase Approach: Application to a Fire Spread Model Across a Fuel Bed. *Combustion Science and Technology*, (in press).

[13] Anderson, H.E. and Rothermel, R.C. (1965) Influence of Moisture and Wind upon the Characteristics of Free-Burning Fires. *10th International Symposium on Combustion*. The Combustion Institute, pp. 1009-1019.

[14] Kolb, G. (1996) Etude d'une flamme non prémélangée caractéristique d'un incendie en présence d'un écoulement forcé. *PHD Thesis*, Université de Poitiers.

[15] Delhaye, J.M. (1976) Local instantaneous equations – instantaneous space – averaged equations – two-phases flow and heat transfer. *Proceedings of NATO Advanced Study Institute*, **1**, Istambul.

[16] Anderson, T. B. and Jackson, R. (1967) A fluid mechanical description of fluidized beds. *Industrial and Engineering Chemistry Fundamentals*, **6**, pp. 527-539.

[17] Drysdale, D. D., Macmillan, A. J. R. (1992) Flame Spread on Inclined Surfaces. *Fire Safety Journal*, **18**, pp. 245-254.

[18] Mendes-Lopes, J.M., Ventura, J.M., and Amaral, J.M. (1998) Rate of spread and flame characteristics in a bed of pine needles. *III Int. Conf. on Fire Research,* **1**, pp. 497-511, Luso.

[19] Weber, R.O. (1989) Analytical models for fire spread due to radiation. *Combustion and Flame*, **78**, pp. 398-408.

[20] Tang, S., S. Qin and R.O. Weber. (1993) Numerical studies on 2-dimensional reaction-diffusion equations. *Journal of the Australian Mathematics Society Series,* **B 35**, pp. 223-243.

[21] Patankar, S.V. (1980) Numerical Heat Transfer and Fluid Flow. *Hemisphere Publishing Corporation*, 198 pages.

[22] Sibony, M., and Mardon J.Cl. (1988) Approximations et équations différentielles. *Hermann Edition*, 475 pages.

[23] Ventura, J. M., Mendes-Lopes, J. M. and Ripado, L.M. (1998) Temperature-time curves in fire propagating in beds of pine needles. *III Int. Conf. on Fire Research,* **1**, pp. 699-711, Luso.

[24] Den Breejen, E., Roos, M., Schutte, K., De Vries, J. S. and Winkel, H. (1998) Infrared measurements of energy release and flame temperatures of forest fires. *III International Conference on Fire Research,* **1**, pp. 517-532, Luso.

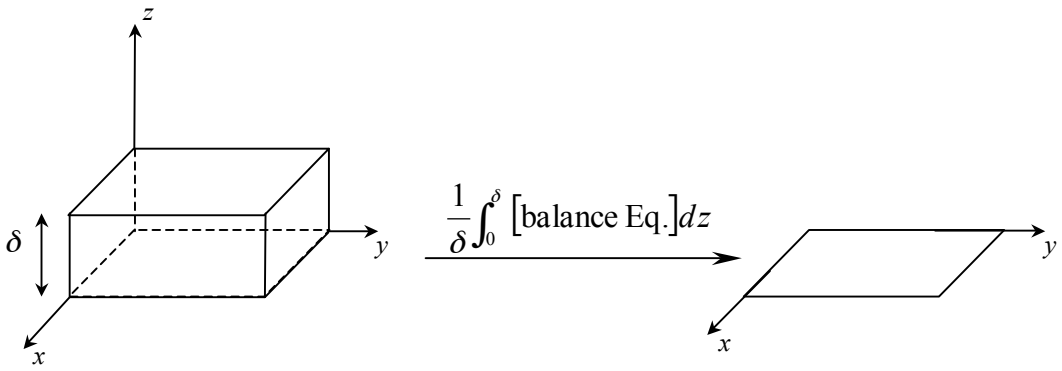

Figure 1. Two dimensional reduction procedure

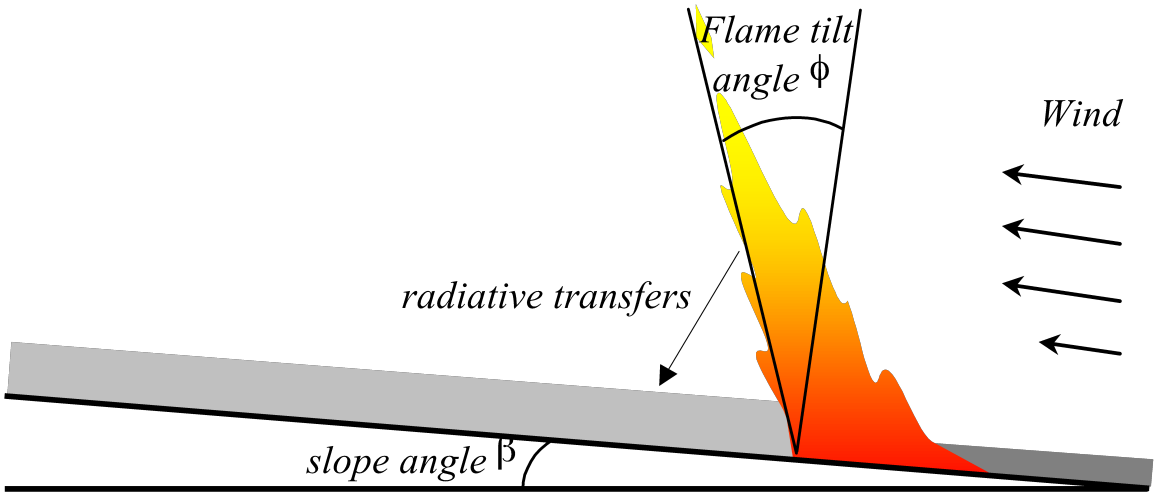

Figure 2. Flame tilt angle under slope and wind conditions

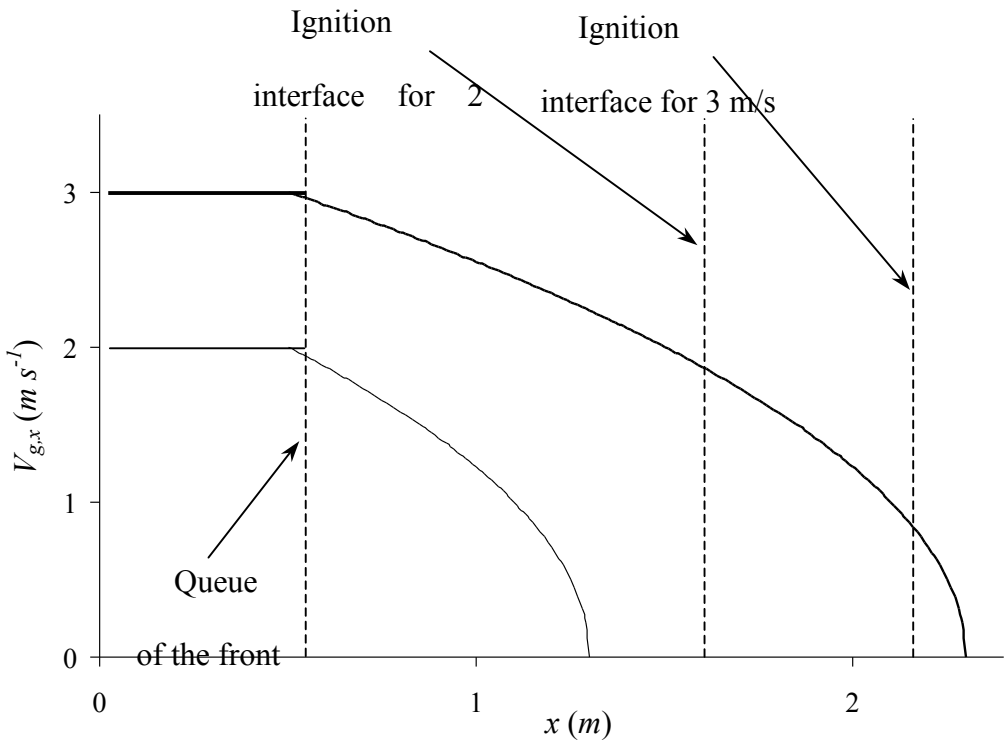

Figure 3. Gas velocity profile along the x direction for wind values of 2 and 3 m s^{-1}

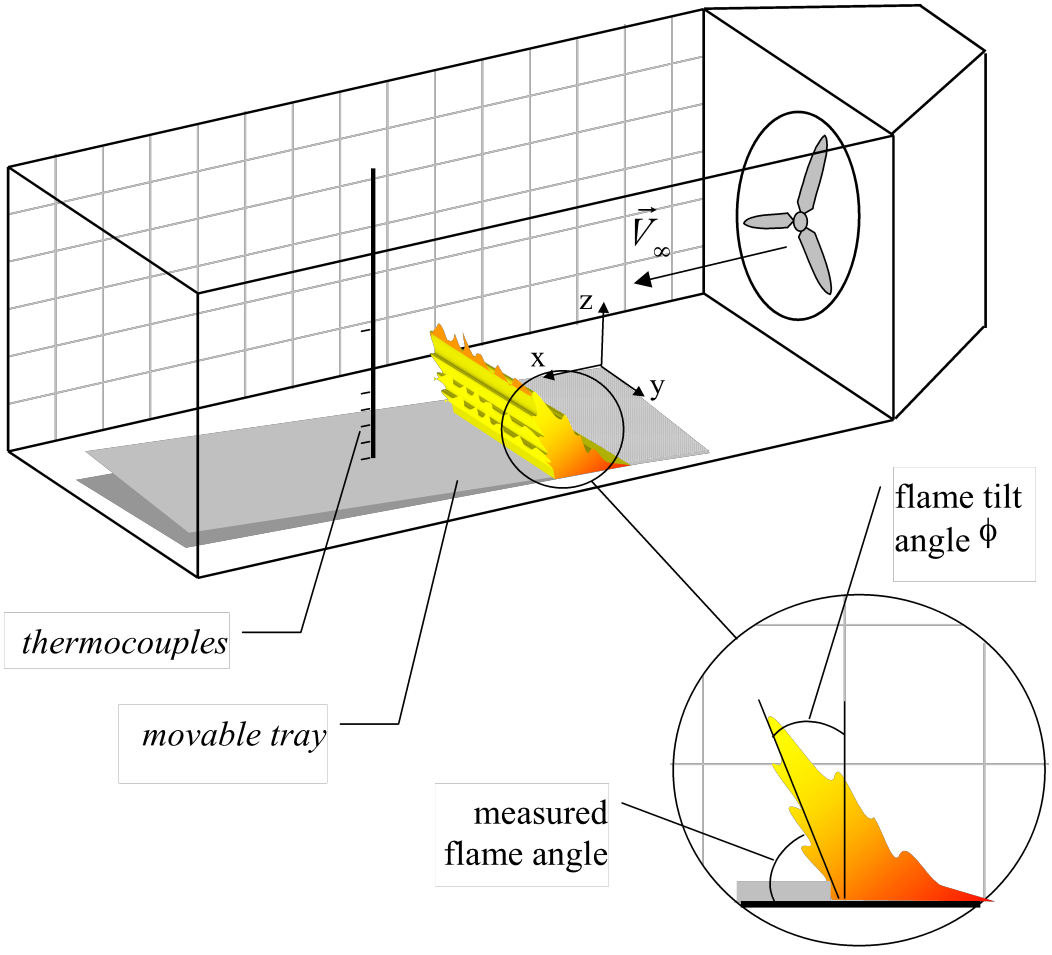

Figure 4. Experimental wind tunnel

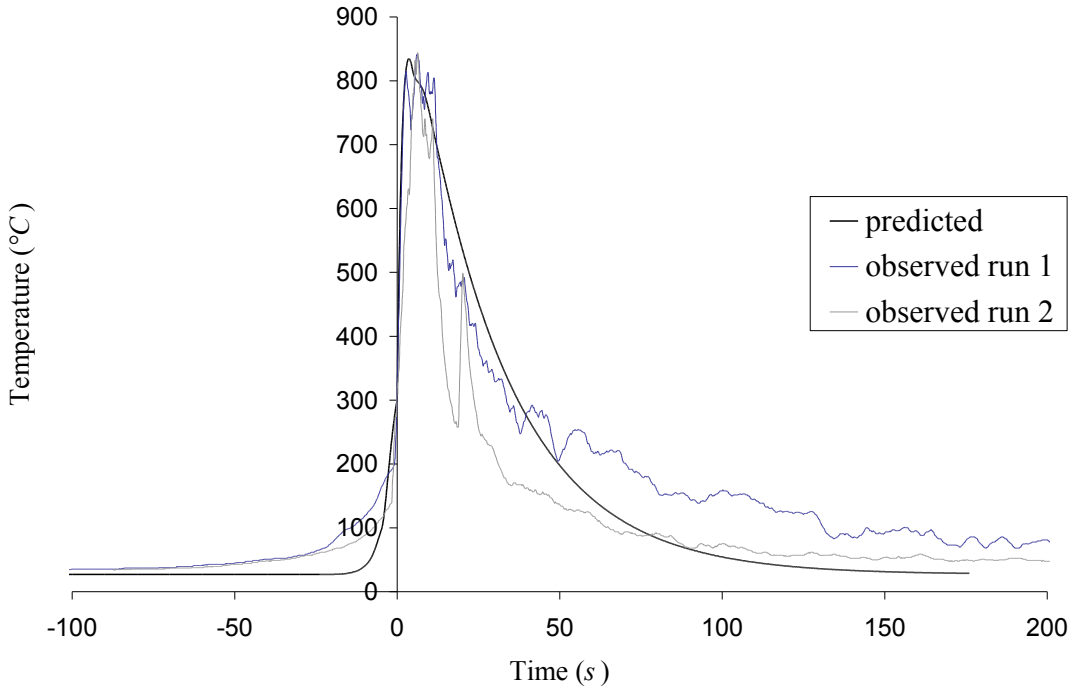

Figure 5. Experimental and predicted temperature curves

in slopeless and windless condition

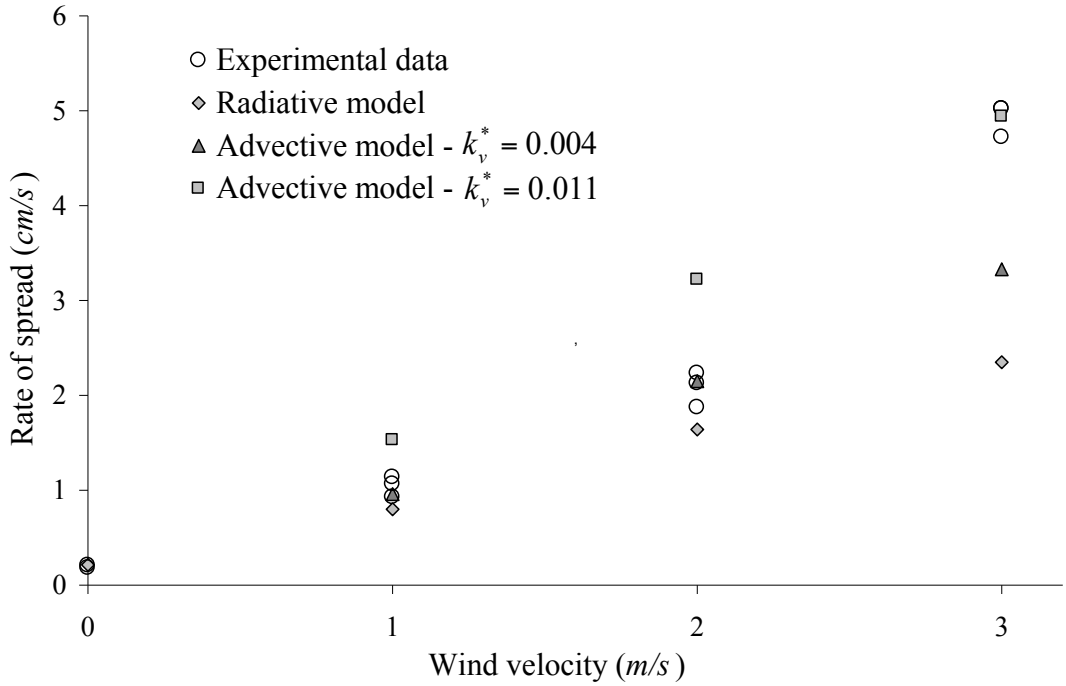

Figure 6. Rates of spread of the radiative and the constant-wind model

for no slope under various wind conditions

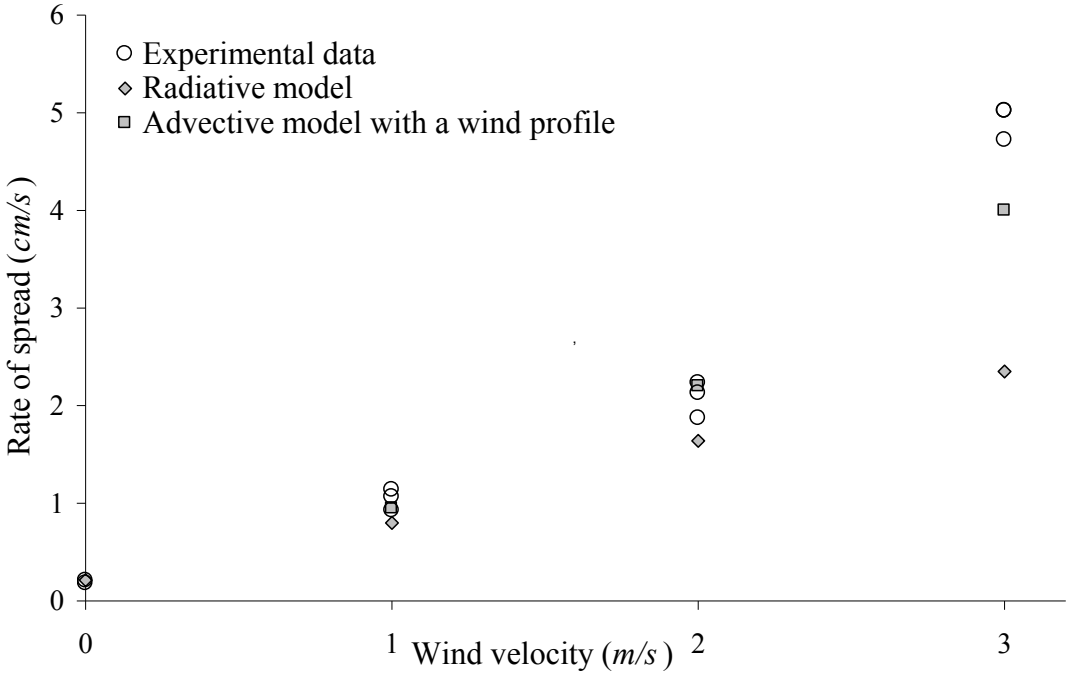

Figure 7. Rates of spread of the improved model including a wind profile

for no slope and under various wind conditions

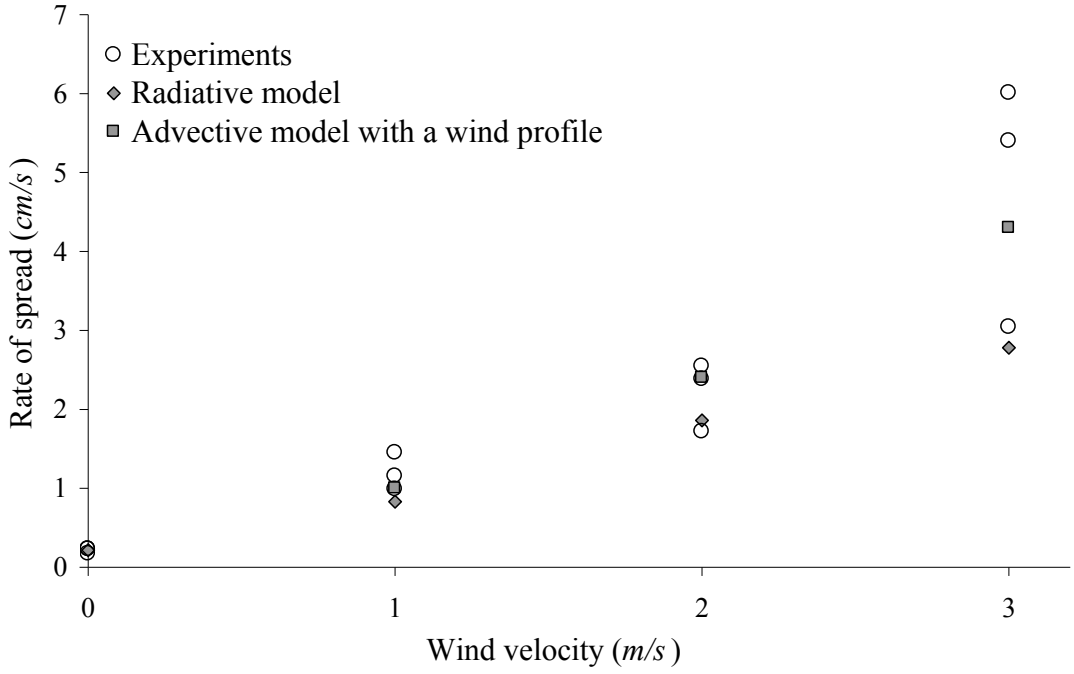

Figure 8. Rates of spread of the improved model including a wind profile

for a 5° slope and under various wind conditions

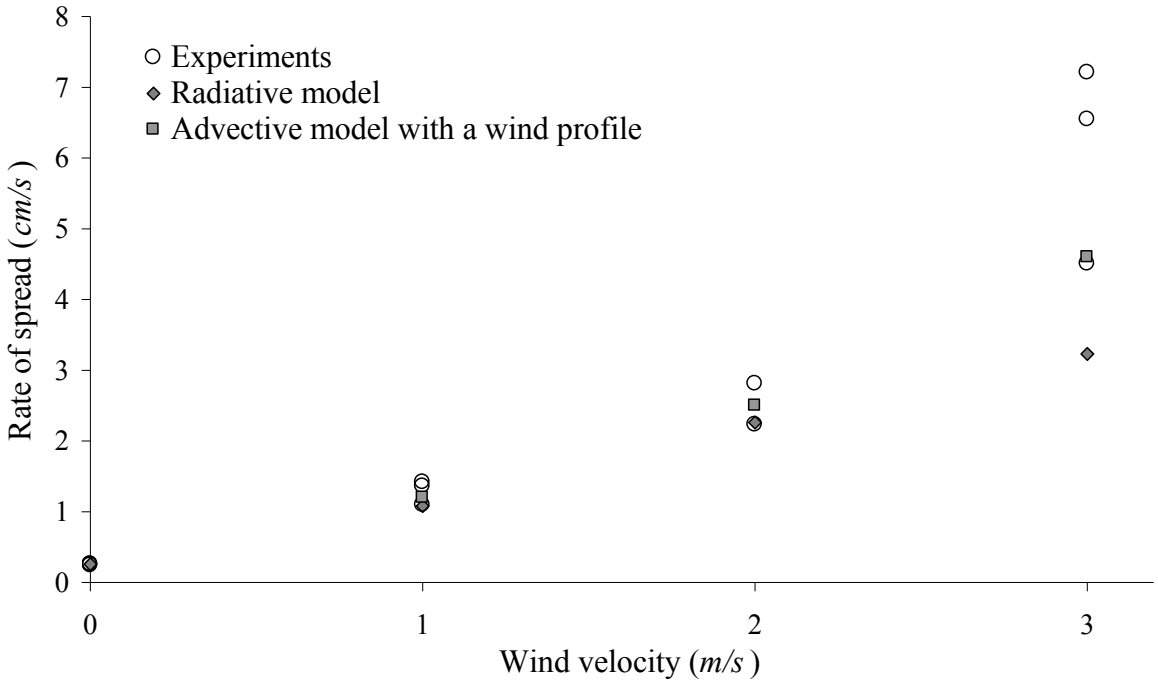

Figure 9. Rates of spread of the improved model including a wind profile

for a 10° slope and under various wind conditions

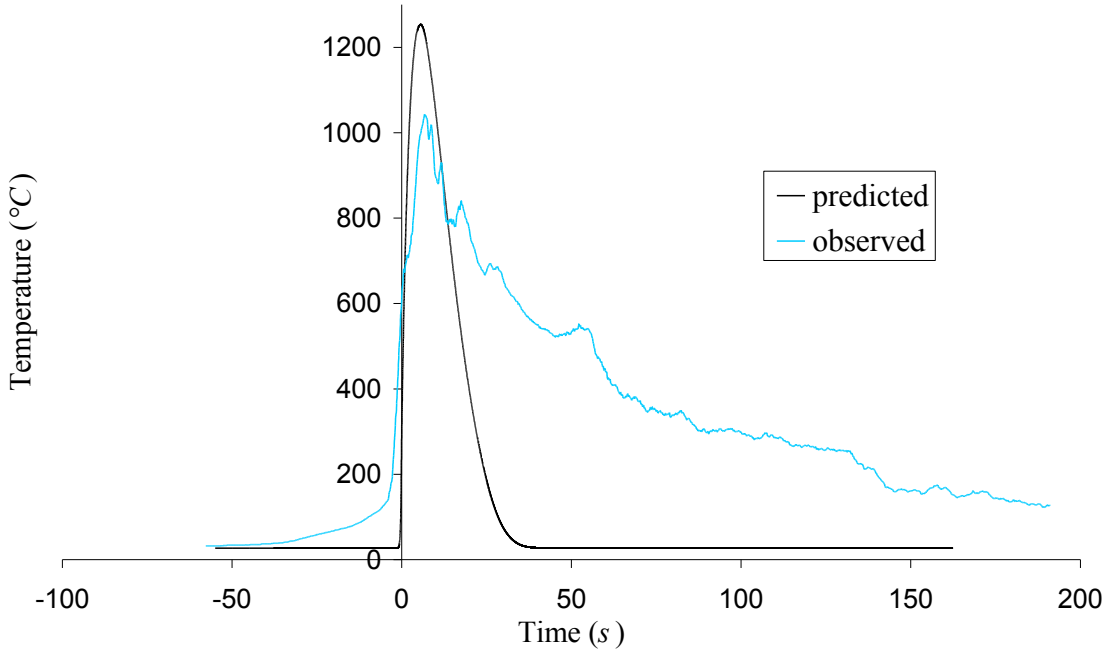

Figure 10. Experimental and predicted temperature curves

for a 10° slope under 2 m s^{-1} wind condition

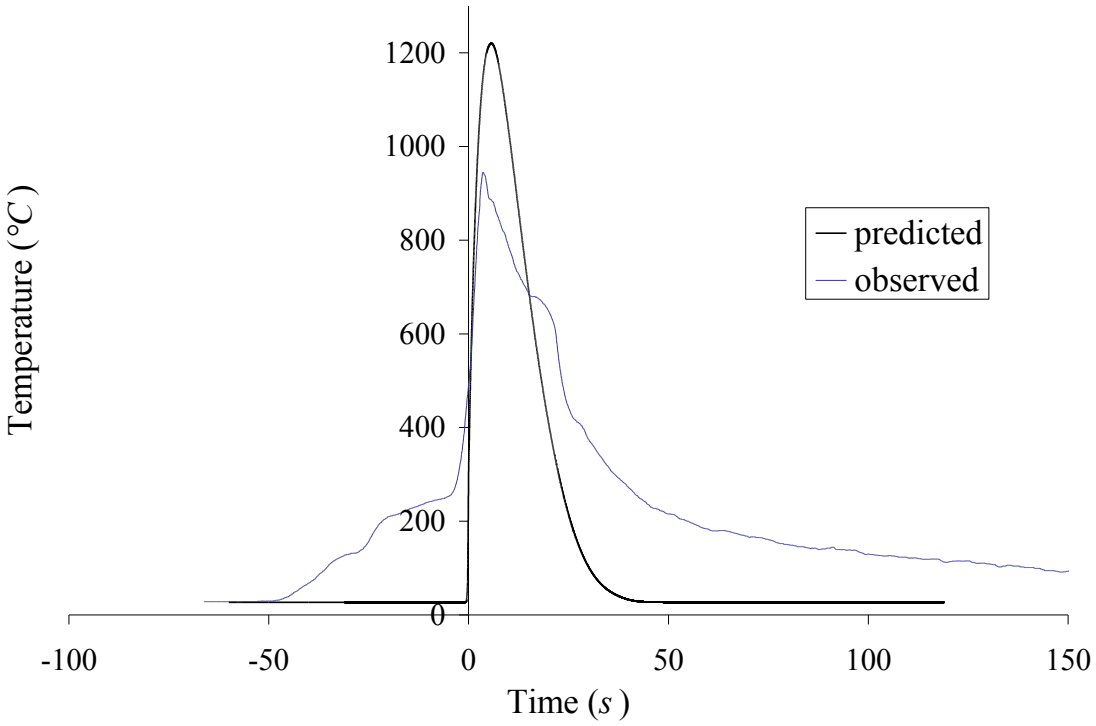

Figure 11. Experimental and predicted temperature curves

for a 10° slope under 3 m s^{-1} wind condition